Preparation, Texture, and Magnetic Properties of Carbon Nanotubes/Nanoparticles Doped with Cobalt

Rohit K. Rana,[†] X. N. Xu,[‡] Y. Yeshurun,[‡] and A. Gedanken*,[†]

Departments of Chemistry and Physics, Bar-Ilan University, Ramat-Gan 52900, Israel

Received: August 27, 2001; In Final Form: January 17, 2002

Formation of cobalt-encapsulating carbon nanotubes/nanoparticles from the decomposition products of $Co(CO)_3NO$ was investigated by carrying out the reaction in a specially arranged closed cell at different temperatures. Multiwalled carbon nanotubes along with carbon-encapsulated cobalt nanoparticles were generated via a catalytic carbon monoxide disproportionation reaction over the in situ formed cobalt nanoparticles on an MgO support. The carbonaceous materials were separated from the product by a simple acid-treatment method. Structure and composition of the products were characterized by X-ray diffraction (XRD), transmission electron microscopy, and thermogravimetric analysis. It was observed that nanotube formation is favored at 1000 °C, whereas lower temperatures produced mainly nanoparticles with or without the encapsulated cobalt. The average outer diameter of the nanotubes was 26 nm with an inner diameter of 15 nm. As revealed from XRD, the encapsulated cobalt particles were in their high-temperature fcc phase and were present at the tip of the nanotubes and inside the nanoparticles. Magnetization measurements showed that the encapsulated cobalt particles are ferromagnetic in nature and the saturation magnetization (M_s) and coercive force (H_c) are dependent on the reaction temperature.

1. Introduction

In the past few years there has been intense research in carbon science, mainly provoked by the discovery of C_{60} in 1985.[1] In a very short period of time, a number of new forms of carbon were identified, such as nested spheroidal shells (onions),[2] giant fullerene shells,[3] interconnected fullerene-like cages,[4] flattened nanotubes, and flattened carbon nanoshells.[5,6] In 1991, another new form of carbon, the carbon nanotubes, was detected by Iijima[7] while investigating the soot obtained from the cathodic deposit of an arc-discharge fullerene production apparatus. The carbon nanotubes are currently an active field of research, owing to their exceptional electrical and mechanical properties, which make them suitable for application in semiconductor devices, field emitters, tunneling microscopes, quantum wires, etc.[8−15]

The carbon nanotubes are unique nanostructures consisting of nested cylindrical graphitic layers capped by fullerene-like ends with a hollow internal cavity. They can be multiwalled or single walled depending on the number of graphitic layers present in the structure. It has also been suggested that nanotubes containing different kinds of materials inside their cores might exhibit interesting properties.[15−17] In particular, for magnetic metal filled carbon nanotubes, the magnetic behavior of the occluded nanoparticles and the oxidation resistance of carbon coating have led to the consideration of these materials for applications in areas such as magnetic data storage, xerography, and contrast agents in magnetic resonance imaging.

Soon after the report of carbon nanotubes by Iijima, many other synthetic methods to produce carbon nanotubes were reported. A lot of effort has been devoted to the synthesis of nanotubes, chiefly because of the requirement in both quantity and quality in order to verify their properties, which were predicted theoretically. All the synthetic methods can be roughly categorized into three groups: the carbon arc-discharge method,[7,8] laser vaporization of a graphite electrode,[18] and chemical methods.[19−23] So far, helium arc discharge is the most widely used fabrication method because of the better quality of the produced nanotubes with well-graphitized tube walls. However, the nanotube sample obtained by this method has the disadvantage of containing other materials, such as graphitic particles. This inhomogeneity of the nanotube samples, as well as the required drastic experimental conditions, has motivated investigations for alternative production techniques. Most of these techniques produce nanotubes through a catalytic process (chemical methods), such as decomposition of hydrocarbons or carbon monoxide over metallic particles. A comparison of the nanotubes prepared by different synthetic techniques showed that the catalytic methods yield nanotubes with many structural defects in the tube walls.[24] However, the lower reaction temperatures involved in these methods, along with the low cost of production, are some of the advantages that have made them an important area of research for the production of nanotubes.

A catalytic method generally involves the decomposition of hydrocarbons or carbon monoxide over a catalyst. From a thermodynamic point of view, the CO decomposition method differs sharply from others (decomposition of hydrocarbons) in that the equilibrium yield of carbon decreases with temperature, whereas it increases for the other cases (e.g., for CO disproportionation, $\Delta G°$(700 K) is −48.4 kJ/mol and $\Delta G°$(900 K) is −12.9 kJ/mol at 1 atm). However, hydrocarbon decomposition has the disadvantage of forming an amorphous carbon coating due to the self-pyrolysis of the reactant at high temperatures. This can be avoided by using CO as the carbon source, as it disproportionates at a sufficiently high temperature to give carbon nanotubes over a catalyst.

* Corresponding author. Fax: +972-3-5351250. E-mail: gedanken@mail.biu.ac.il.
[†] Department of Chemistry.
[‡] Department of Physics.

10.1021/jp013320t CCC: $22.00
Published on Web 03/30/2002

Several studies on the catalytic disproportionation of CO for the production of nanotubes have been reported. Dai et al. were the first to prepare SWNT by a preformed catalyst from a flow of CO gas.[25] Tube diameters ranging from 1 to 5 nm were produced over Mo particles for which they proposed a "skull-cap" type of growth mechanism. The nano-sized Mo particles were responsible for the nanotube formation, whereas the larger Mo particles were found to be fully covered by graphitic layers and were thus inactive in catalyzing the tube formation. A comparative microscopic study on the products obtained from catalytic decomposition of CO over a catalyst (Fe, Co, and Ni) and high-temperature arc-discharge method showed that the materials produced from both methods have similar morphologies.[26] They also showed that the presence of hydrogen could influence the process to give carbon filaments instead of nanotubes. The various other catalysts, which were employed for the synthesis of nanotubes from CO decomposition, are Ni−MgO,[27] Co−Mo,[28] and Co−Al_2O_3.[29] In all the above methods, the catalysts were prepared prior to their use in the nanotube fabrication, and in some cases the effects of catalyst preparation on nanotube growth were also investigated in detail.

Recently, it has been shown by our group that metal carbonyls can be employed as the source for both carbon monoxide and catalyst where the nanotubes grow from the in situ generated metal catalysts.[30−32] Carbon "nanoflasks" having circular or ovoid bulb-type bases with long nanotube necks were obtained when the metal carbonyl, along with magnesium, was heated in a closed cell at 900−1100 °C. Here we describe a method by which multiwalled carbon nanotubes and nanoparticles were obtained from the decomposition products of $Co(CO)_3NO$ when the reaction was performed over MgO or a mixture of Mg and MgO instead of only Mg. A detailed study on the effect of various experimental conditions upon the morphology of the formed products and their magnetic properties has been discussed. A short communication of the early results has been published recently.[33]

2. Experimental Section

Syntheses of carbon nanotubes were carried out in a 2 mL closed cell, which was assembled from stainless steel Swagelok parts. A 3/8 in. union part was capped from one side by a standard plug. For dispersing the generated metal particles from the decomposition of metal carbonyl, we used a mixture of Mg and MgO. This is based on the fact that the reactivity of MgO can be enhanced by exposure of the sample to vapors of low ionization energy metals such as magnesium and alkali metals, and thereby change its catalytic properties.[34,35] In a typical preparation method, 350 mg of MgO (Merck, BET surface area = 52 m^2/g) mixed with 75 mg of Mg turnings (Merck) was loaded into the cell, and 700 mg of cobalt tricarbonyl nitrosyl (STREM) was added to it slowly by a syringe. The cell was then closed with the other plug. Prior to the loading, MgO powder was heat treated at 500 °C in an atmosphere of nitrogen for 3 h and loading of the cell was carried out in an inert atmosphere of nitrogen (glovebox). The filled cell was then heated in a furnace to the desired temperature at a heating rate of 20 °C/min. The reaction was continued for different durations, after which the cell was cooled to room temperature. The as-synthesized black product obtained from the cell was treated with 30% dilute HCl solution to remove the catalytic particles. The resulting purified material was centrifuged, repeatedly washed with deionized water and ethanol, and then vacuum-dried. The products are designated as C_x, where x represents the reaction temperature.

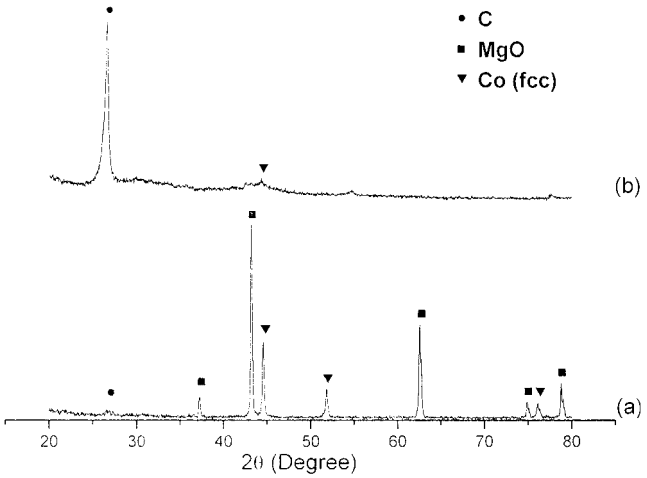

Figure 1. X-ray diffractograms of (a) as-synthesized and (b) acid-treated C_{1000} sample.

The X-ray diffraction patterns of the products were recorded by employing a Bruker AXS D8 Advance Powder X-ray Diffractometer (using Cu Kα $\lambda = 1.5418$ rad). The transmission electron micrographs (TEM) were obtained with a JEOL-JEM 100SX microscope, working at a 100 kV accelerating voltage. Samples for TEM were prepared by dispersing the powdered sample in ethanol by sonication and then drop-drying on a copper grid (400 mesh, Electron Microscopy Sciences) coated with carbon film. The TGA measurements were carried out under air on a Mettler Toledo TGA/SDTA 851 instrument at a heating rate of 5 °C/min. Elemental analysis was done by an Eager 200 CHN analyzer. Magnetization was measured using a vibrating sample magnetometer (VSM-Oxford 3001).

3. Results and Discussion

3.1. XRD Analyses. The different phases in the as-synthesized and acid-treated samples were characterized by XRD. Figure 1 illustrates the XRD patterns of the C_{1000} sample before and after acid treatment. In the case of the as-synthesized sample, the pattern mainly consists of dominating peaks due to MgO. The other less intense peaks could be assigned to metallic cobalt particles and graphite. The Co particles were found to be in their unstable fcc phase. The stabilization of the fcc structure rather than the stable hcp phase was similar to that in our earlier report.[30] It was proposed that the covering graphene layers could be responsible for the stabilization of the fcc phase. After the sample was acid treated, the (002) graphitic peak became more prominent. In addition, the dominant MgO peaks disappeared due to the removal of the MgO particles by HCl. From the graphitic (002) peak the average interlayer spacing was calculated to be 3.4 Å, which is less by 0.04 Å than the reported value for carbon nanotube/nanoparticle mixtures obtained by the arc-discharge method.[36] However, it is known from the more recent analysis by Kiang et al.[37] that the interlayer spacing can vary from 3.4 to 3.9 Å depending on the tube diameter, with the smaller diameter tubes having the largest spacing. This correlation was attributed to the high curvature of the small tubes resulting in a greater repulsive intertube force.

As seen from the diffraction pattern in Figure 1b, a small amount of Co was found to remain even after the acid treatment. These Co particles are still in their fcc symmetry, suggesting that they are strongly covered by the graphene layers, which prevented the metal from reacting with HCl. The XRD patterns of the C_{800} and C_{900} samples are shown in Figures 2 and 3. Patterns of all the samples are similar to those of C_{1000} except

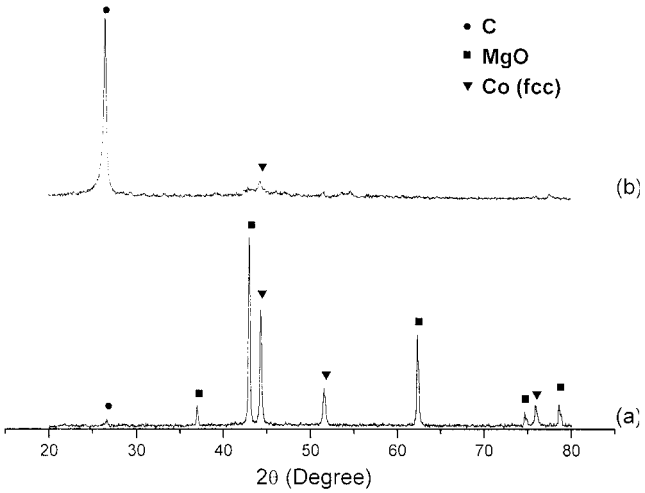

Figure 2. X-ray diffractograms of (a) as-synthesized and (b) acid-treated C_{900} sample.

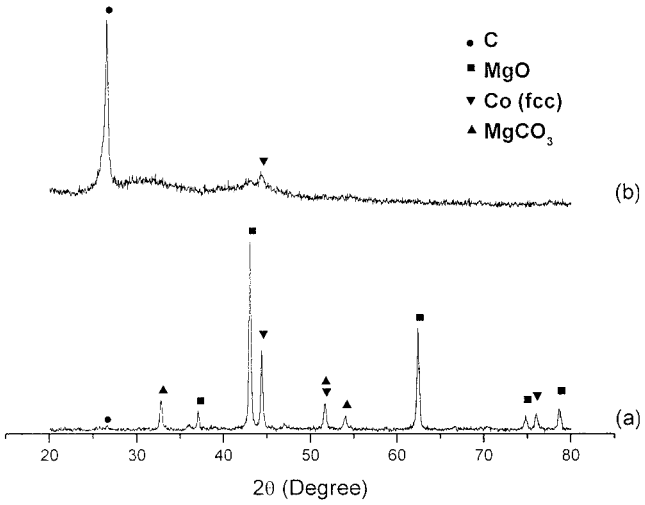

Figure 3. X-ray diffractograms of (a) as-synthesized and (b) acid-treated C_{800} sample.

the as-synthesized C_{800} sample, for which extra peaks due to $MgCO_3$ were observed. The presence of $MgCO_3$ only for the sample prepared at 800 °C indicates that this might have formed from the reaction of CO_2 on the surface of MgO, and on further heating to higher temperature it decomposes. The *d* spacings for the graphitic (002) peak for C_{800} and C_{900} samples are 3.35 and 3.36 Å, respectively, and are similar to that of a graphite crystal (3.354 Å).

3.2. CHN Analyses. Carbon contents in various samples were determined by CHN analysis. The as-synthesized C_{1000} sample obtained after 3 h of reaction showed a carbon content of 6.4 wt %. In good agreement with this, the amount of material that was recovered from the products after treating with HCl corresponded to about 6.8 wt % of the as-synthesized product. The balance of weight shows the effectiveness of the purification method, which caused removal of the catalytic materials only. The percentage of carbon yield could be estimated from this, and it corresponds to about 32.1 wt % of the total amount of carbon that was initially present in the reaction mixture. In the acid-treated sample, the carbon content was 95 wt % and the contents of the other elements such as H, N, and O were below 1 wt %.

The carbon yields for all the as-synthesized products obtained at various times and temperatures are listed in Table 1. A very slow increase in the carbon content with time was observed for

TABLE 1: Carbon Yields for Various As-Synthesized Samples and Cobalt Content in Acid-Treated Samples

sample	reaction temp (°C)	reaction duration (h)	carbon yield (wt %)	wt % Co[a]
C_{1000}	1000	1	29.8	
		3	32.1, 16.8[b]	4.9
		7	34.8	
		10	35.2	
C_{900}	900	3	39.3	6.0
C_{800}	800	3	44.8	6.5
$Co(CO)_3NO$	1000	3	12.7	

[a] Cobalt contents in the acid-treated samples calculated from TGA analyses. [b] The value corresponds to percentage of carbon yield for the product obtained in the absence of magnesium.

the reaction at 1000 °C. It can be seen that most of these carbons have already been formed at 1 h. When the reactions were performed at lower temperatures (800 and 900 °C), they produced more carbon corresponding to 44.8 and 39.3 wt % yields, respectively. This may be the consequence of the decrease in free energy change (ΔG for the CO disproportionation reaction) with temperature making the reaction more favorable at lower temperatures, thus yielding a higher amount of product. Moreover, in the case of C_{800}, the formation of $MgCO_3$ also adds to the total amount of carbon present in the as-synthesized product. For comparison, the carbon content in the product obtained by heating only $Co(CO)_3NO$ inside the cell at 1000 °C is also given in Table 1. The lower percentage of conversion in this reaction can be related to the lower activity of bigger metal particles (≥500 nm) formed from the decomposition of $Co(CO)_3NO$ in the absence of any support.

The advantage of using Mg along with MgO was reflected in the increase in carbon yield from a value of 16.8 wt % for MgO to 32.1 wt % for a mixture of Mg and MgO. This indicates that Mg plays an important role in promoting the reaction over cobalt catalyst. The promotional effect can be directly due to the interaction of either Mg with cobalt or through a metal/support interaction. We assume that Mg can promote the reaction in a manner similar to that known in the case of alkali metal promoted Fischer−Tropsch catalysis.[38,39] Various experiments and theoretical calculations have shown that the interaction of electropositive adatoms such as Na or K with the transition metal surface causes an enhancement of the binding energy of molecularly adsorbed CO and increases the dissociation probability of CO.[38−41] This has been attributed to the increased electron density on the transition metal surface atoms by the adsorption of alkali metal atoms on them. On the other hand, Mg may also indirectly promote the cobalt catalyst through an interaction with the MgO support. It has been shown that when MgO is exposed to Mg vapor, it generates an electron-rich surface by creating defect centers consisting of single electrons in anionic vacancies.[34,42] This electron rich defect site can activate the cobalt catalyst by donating electrons through metal/support interaction.

3.3. TEM Analyses. Representative TEM images of the as-synthesized and the extracted products are illustrated in Figures 4 and 5. As seen in Figure 4a, only a few carbon nanotubes could be detected in the as-synthesized material and most of them were covered with the catalytic particles. However, these impurities were not seen in the case of the HCl-treated product and the nanotubes were clearly visible, as shown in Figure 4b−d. The morphologies of the nanotubes before and after the acid treatment remained similar, indicating that they are undamaged by this purification method. The dimensions of carbon nanotubes were varied in a narrow size range with an outer diameter of ∼26 nm for most of them, and the rest had a diameter in the

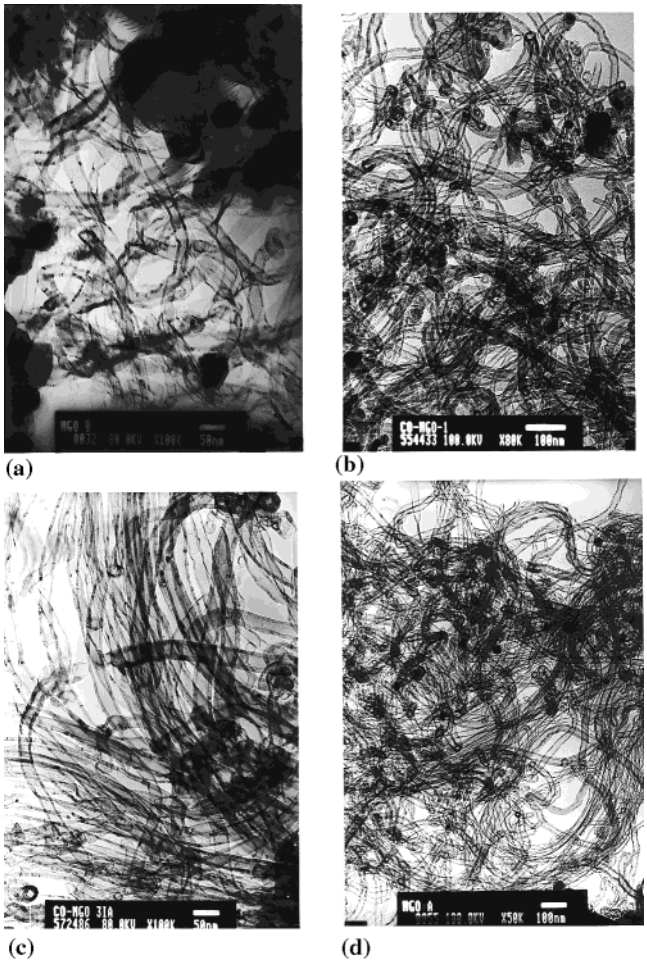

Figure 4. Transmission electron micrographs of (a) as-synthesized material and (b, c, and d) acid-treated samples obtained from the reaction at 1000 °C for 1, 3, and 7 h durations, respectively.

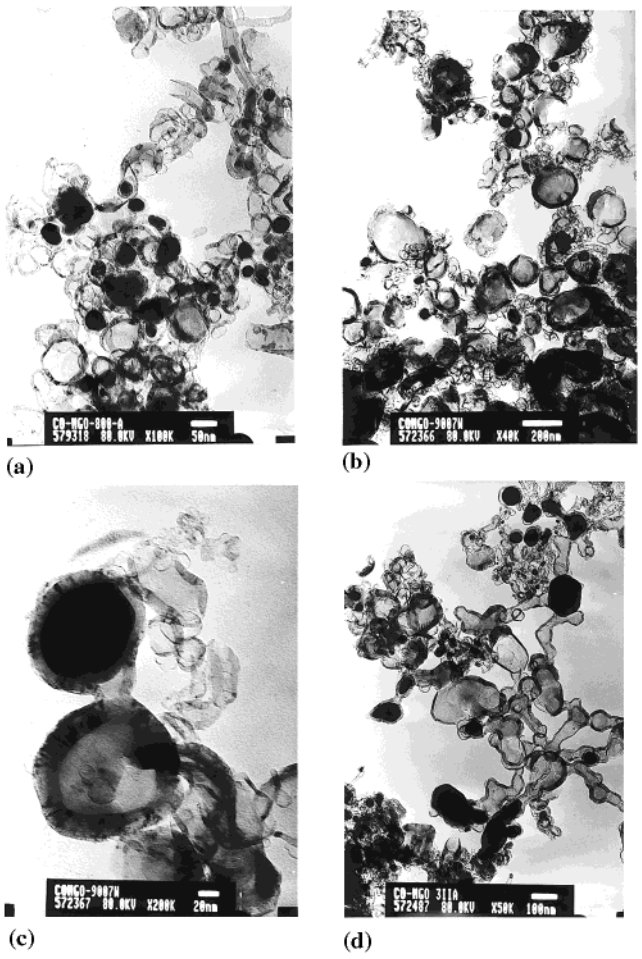

Figure 5. Transmission electron micrographs of acid-treated samples obtained at (a) 800, (b, c) 900, and (d) 1000 °C (heating rate 100 °C/min).

16−34 nm range. The distribution of the inner diameters was in the 10−22 nm range with an average of ∼15 nm. Accordingly, the tube-wall thickness varied from 3 to 10 nm with the majority of the tubes consisting of about ∼15 graphitic layers, corresponding to a wall thickness of ∼6 nm. The nanotubes with larger diameters were often found to have thicker walls. It was also observed that many of the nanotubes were attached with very small cobalt particles of 20−35 nm size (Figure 4b,c) at one of their ends. The similarity in the size of these encapsulated cobalt particles and the outer diameters of the attached tubes clearly indicates that the dimensions of the nanotubes are determined by the size of the catalytic particles.

Although the carbon content in the C_{1000} product was found to increase with time (Table 1), there was not much change in the nanotube content (Figure 4b−d). Since all of the metal carbonyls must have decomposed well before the reaction temperature reached 1000 °C, and all the formed metal particles suitable for the nanotube growth might have been covered with carbon at the initial stages of the reaction, one cannot expect any further generation of new nucleating centers for the nanotube growth at later times. Thus, the extra carbon that was being formed at later hours might be contributing to the further growth of the tubes that had already been nucleated at the beginning of the reaction.

To understand the effect of reaction temperature on the product morphology, the products obtained from the reactions at 800 and 900 °C were also analyzed by TEM. For both temperatures the overall nanotube content was decreased drastically producing mainly nanoparticles. As shown in Figure 5a−c, the C_{900} sample has comparatively bigger particles than C_{800}, and for both cases it has a wide size distribution ranging from 50 to 200 nm. Many of these nanoparticles have an empty core, while the others have encapsulated metal particle. In the case of hollow particles, the empty core is a result of the removal of metal particles during the acid-treatment procedure. For the encapsulated particles, because of the surrounding graphene layers the metal was well protected from leaching out by HCl. However, the low content of the nanotubes at these temperatures was in contradiction to the other reported results where nanotubes were observed even below 700 °C from a continuous flow of CO over a catalyst.[43] This can be attributed to the lower ratio of CO to metal in our case, which allows the metal particles to agglomerate, forming bigger particles at 800 °C and 900 °C, thus making them inactive for the nanotube nucleation. When catalytic particles become larger, the formation of graphitic overcoat is favored, as the strain energy of the over-coating layer becomes smaller.[44] However, in case of the reaction at 1000 °C, because of the enhanced reactivity for nanotube formation, the initially formed smaller metal particles start nucleating the nanotubes before reacting with other metal particles to form bigger aggregates. Thus, it can be said that the product formation is mainly directed by competition between two reactions, i.e., nanotube formation and agglomeration of the metal particles. It was also observed that the nanotube content decreased by increasing the rate of heating, further suggesting that the higher rate of heating facilitated the agglomeration of metal particles, resulting in nanoparticles only (Figure 5d).

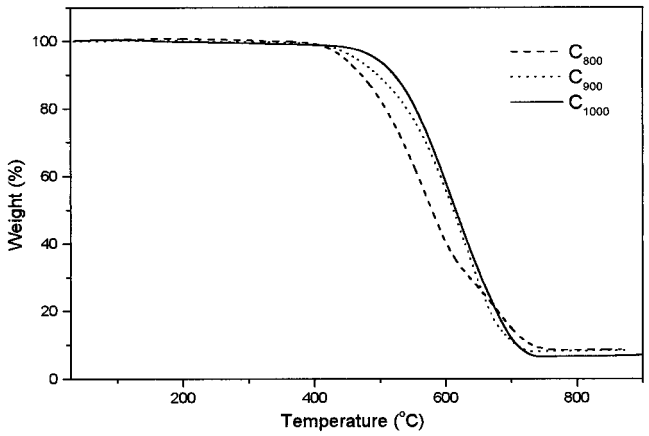

Figure 6. TGA curves for acid-treated samples of C_{1000}, C_{900}, and C_{800}.

3.4. Mechanism. The nanotube tips containing Co particles as seen from the TEM images reveal that these small metal particles are responsible for the nucleation and growth of nanotubes. First, the decomposition of metal carbonyl over MgO gives rise to nanosized metal particles and carbon monoxide. These cobalt nanoparticles then catalyze the disproportionation of carbon monoxide to form carbon over the metal particles from which the nucleation and growth of carbon nanotube takes place. The trapped cobalt particles seen in the tip of the nanotubes are similar to that already reported for both SWNT and MWNT syntheses.[23,25] Thus in our case we anticipate a similar "yarmulke" type of catalytic mechanism as has been proposed earlier.[25] According to this mechanism, an excess of carbon assembles on the metal particle surface to form a graphene cap with its edges strongly chemisorbed to the metal. The newly arriving carbon then either forms another cap underneath the first or adds to the cylindrical section of a growing layer to form a tubular structure with one of its ends still attached to the metal particle.

3.5. TGA Analyses. Thermogravimetric analyses were carried out in order to quantify the nanoparticle/nanotube contents in acid-treated samples. TGA curves for the samples prepared at three different temperatures are shown in Figure 6. For all samples, weight loss starts at ~400 °C and continues until ~750 °C. It is known that the nongraphitic carbon oxidizes first at a temperature below 550 °C.[45] Above 550 °C the weight loss is related to the oxidation of carbon nanotubes/nanoparticles. However, the reported onset value for multiwalled carbon nanotubes prepared by the arc-discharge method is ~700 °C,[46] which is higher than that found in our study. This decrease in the decomposition temperature could be due to the presence of metal particles in the sample, which can catalyze the oxidation of carbon nanotubes at a lower temperature.[46] Moreover, the exothermic reaction of the first component can also initiate burning of the second component at a lower temperature.[47] From the TGA curve, the total nanotube and nanoparticle content in C_{1000} was estimated to be 73 wt %. The values for C_{800} and C_{900} are 62 and 70 wt % respectively, which indicates that at lower temperatures the formation of nongraphitic carbon is favored as compared to that at 1000 °C. The metal content in various samples was also calculated from the residue by considering it as completely oxidized, and is given in Table 1.

3.6. Magnetic Measurements. Carbon encapsulation of the magnetic materials is of importance as the effective distance of neighboring magnetic grains can be increased so as to weaken or eliminate the exchange coupling between them. Carbon encapsulation can also provide protection against surface oxidation of magnetic grains. These magnetic nanoparticles are generally prepared by the high-temperature carbon-arc technique, the tungsten-arc technique, the Magnetron and ion-beaming technique, and the rf plasma torch technique. The cobalt-containing carbon nanotubes/nanoparticles produced by our chemical method may provide an alternative route for their preparation in a comparatively low temperature region.

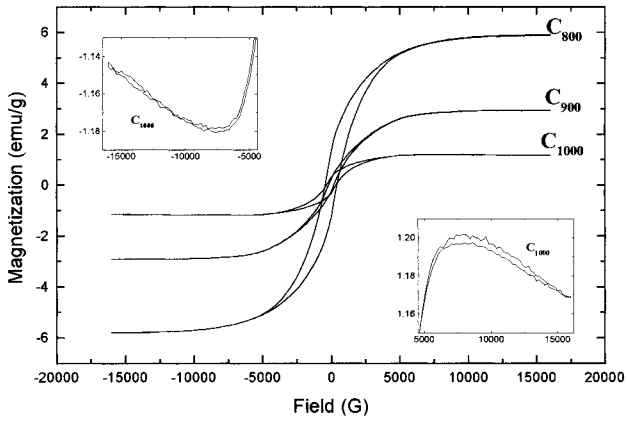

Figure 7. Plot of magnetization vs applied field for various samples measured at 300 K. Inset figures show the magnified parts of the curve for C_{1000} in high magnetic field region.

TABLE 2: Magnetization Data for Various Samples Measured at 300 K

sample	M_s (emu/g)	M_r/M_s	H_c (G)	M_s (emu/g of Co)
C_{800}	5.8	0.2	435	90
C_{900}	2.9	0.1	197	49
C_{1000}	1.2[a]	0.3	302	24

[a] The saturation value corresponds to the highest value achieved (at 8000 G) before the diamagnetic decrease of magnetization with applied field.

Magnetic properties of the samples were investigated at room temperature using a vibrating sample magnetometer with an applied field $-1.6\ \text{T} \le H \le 1.6\ \text{T}$. Plots of magnetization vs applied magnetic field for various samples are given in Figure 7. In the case of C_{1000}, a typical ferromagnetic behavior was observed at low field range, and after 8000 G the behavior became diamagnetic with negative magnetic susceptibility (see inset of Figure 7). Although the pure carbon nanotubes are known to exhibit a greater diamagnetic susceptibility compared with graphite,[48] this decrease is also in the same range that can be expected from the diamagnetic contribution of a sample holder. Thus, the decrease in magnetization with the applied magnetic field above 8000 G is indicative of an additive effect of ferromagnetic saturation of cobalt magnetization and a diamagnetic decrease in the magnetization of carbon nanotubes and/or the sample holder with increasing field. Magnetization curves for C_{800} and C_{900} reveal that these samples are also ferromagnetic in nature, but in contrast to the diamagnetic character of C_{1000} at higher field, the magnetization attained saturation values above 8000 G. The absence of diamagnetic contribution in C_{800} and C_{900} can be attributed to the lower percentage of carbon nanotubes as evidenced in the TEM pictures.

Values of saturation magnetization, remanence-to-saturation ratio, and coercive field for all samples are listed in Table 2. The coercive force changes with reaction temperature in the following order: $C_{800} > C_{1000} > C_{900}$. This trend can be well correlated to the sizes of the cobalt particles. The coercive force is known to follow a peak with increase in particle size, and at a critical size it attains the maximum value.[49] Thus, the C_{1000} sample having the smallest cobalt particles belongs to the left

side of the peak, where the particles are of a single domain system. Similar coercive forces were also reported by Block et al.[50] and Saito et al.[51] for graphite-coated Co particles of 5−50 and 10−100 nm size, respectively, prepared by an arc-discharge process. In the case of C_{800} and C_{900}, as they have comparatively bigger particles, their behavior can be related to that of multidomain systems placed on the right side of the peak with C_{800} near the maximum and C_{900} (larger particles) with a lower coercivity. In contrast to the size dependence of coercive force, the saturation magnetization was found to follow a different order: $C_{1000} < C_{900} < C_{800}$. This contradicting behavior, however, cannot be explained on the basis of particle size only. Any explanation at this point will be arbitrary, and it requires further investigation, which is currently in progress.

4. Conclusions

Cobalt-encapsulating carbon nanotubes and nanoparticles are formed from the decomposed products of $Co(CO)_3NO$ over a mixture of Mg and MgO via catalytic disproportionation of carbon monoxide. By a variation in the reaction temperature, it was possible to control the morphology and composition of the final product. Nanotubes are favorably generated at a reaction temperature of 1000 °C, whereas lower temperatures produce mainly nanoparticles. Uniformly dispersed small metal particles formed on the support are the active centers for nucleation and growth of nanotubes, which also result in a narrow size distribution for the generated nanotubes. If Mg is used along with MgO, the overall carbon yield is increased as a result of a promotional effect on the cobalt catalyst. Moreover, the use of MgO as the support is advantageous for its effectiveness in dispersing the metal particles, in addition to its easier removal by a simple acid-treatment method.

The nanoparticles are formed with or without the encapsulated cobalt particles. These cobalt particles, which are also present at the tips of nanotubes, are stabilized in fcc phase by the graphite coating. Magnetic measurements showed that the encapsulated cobalt particles are ferromagnetic in nature and the saturation magnetization (M_s) and coercive force (H_c) can be altered significantly with change in reaction temperature. The smaller cobalt particles encapsulated at the tip positions of nanotubes show single domain behavior with a high coercive force. On the other hand, the nanoparticles obtained at lower temperatures are of multidomain systems. The above results evidently demonstrate that the chemical method employed here is promising for fabricating carbon-coated cobalt particles at lower temperatures.

Acknowledgment. We thank the Israeli Ministry of Science, Culture and Sports for supporting this research via an Infrastructure grant. R.K.R. thanks the Bar-Ilan Research Authority for his postdoctoral fellowship. A.G. thanks the German Ministry of Science through the Deutsche−Israel program, DIP, for its support. The authors are grateful to Prof. Z. Malik, Faculty of Life Sciences, for extending to us the use of their facilities.

References and Notes

(1) Kroto, H. W.; Heath, J. R.; O'Brien, S. C.; Curl, R. F.; Smalley, R. E. *Nature* **1985**, *318*, 162.
(2) Ugarte, D. *Nature* **1992**, *359*, 707.
(3) Bourgeois, L. N.; Bursill, L. A. *Philos. Mag. A* **1997**, *76*, 753.
(4) Iijima, S.; Wakabayashi, T.; Achiba, Y. *J. Phys. Chem.* **1996**, *100*, 5839.
(5) Chopra, N. G.; Benedict, L. X.; Crespi, V. H.; Cohen, M. L.; Louie, S. G.; Zettl, A. *Nature* **1995**, *377*, 135.
(6) Bourgeois, L. N.; Bursill, L. A. *Chem. Phys. Lett.* **1997**, *277*, 571.
(7) Iijima, S. *Nature* **1991**, *354*, 56.
(8) Ajayan, P. M. *Chem. Rev.* **1999**, *99*, 1787.
(9) Saito, R.; Fujita, M.; Dresselhaus, G.; Dresselhaus, M. S. *Mater. Sci. Eng., B* **1993**, *19*, 185.
(10) Hamada, N.; Sawada, S.-I.; Oshiyama, A. *Phys. Rev. Lett.* **1992**, *68*, 1579.
(11) Dekker, C. *Phys. Today* **1999**, May, 22.
(12) Dai, H.; Hafner, J. H.; Rinzler, A. G.; Colbert, D. T.; Smalley, R. E. *Nature* **1996**, *384*, 147.
(13) de Heer, W. A.; Bonard, J.-M.; Fauth, K.; Chatelain, A.; Forro, L.; Ugrate, D. *Adv. Mater.* **1997**, *9*, 87.
(14) Wong, E. W.; Sheehan, P. E.; Lieber, C. M. *Science* **1997**, *277*, 1971.
(15) Majetich, S. A.; Artman, J. O.; McHenry, M. E.; Nuhfer, N. T.; Staley, S. W. *Phys. Rev. B* **1993**, *48*, 16845.
(16) Seraphin, S.; Zhou, D.; Jiao J. *J. Appl. Phys.* **1996**, *80*, 2097.
(17) Harris, P. J. F.; Tsang, S. C. *Carbon* **1996**, *34*, 1859.
(18) Thess, A.; Lee, R.; Nikolaev, P.; Dai, H.; Petit, H.; Robert, J.; Xu, C.; Lee, Y. H.; Kim, S. G.; Rinzler, A. G.; Colbert, D. T.; Scuseria, G.; Tomanek, D.; Fischer, J. E.; Smalley, R. E. *Science* **1996**, *273*, 483.
(19) Baker, R. T. K.; Barber, M. A.; Barber, P. S.; Harris, P. S.; Feates, F. S.; Waite, R. J. *J. Catal.* **1972**, *26*, 51.
(20) Yacaman, M. J.; Yoshida, M. M.; Rendon, R.; Santiesteban, J. G. *Appl. Phys. Lett.* **1993**, *62*, 202.
(21) Hsu, W. K.; Hare, J. P.; Terrones, M.; Kroto, H. W.; Walton, D. R. M.; Harris, P. J. F. *Nature* **1995**, *377*, 687.
(22) Pigney, A.; Laurent, Ch.; Dobigeon, F.; Rousset, A. *J. Mater. Res.* **1997**, *12*, 613.
(23) Colomer, J.-F.; Piedigrosso, P.; Willems, I.; Journet, C.; Bernier, P.; Van Tendeloo, G.; Fonseca, A.; Nagy, J. B. *J. Chem. Soc., Faraday Trans.* **1998**, *94*, 3753.
(24) Bulusheva, L. G.; Okutrub, A. V.; Asanov, I. P.; Fonseca, A.; Nagy, J. B. *J. Phys. Chem. B* **2001**, *105*, 4853.
(25) Dai, H.; Rinzler, A. G.; Nikolaev, P.; Thess, A.; Colbert, D. T.; Smalley, R. E. *Chem. Phys. Lett.* **1996**, *260*, 471.
(26) Jiao, J.; Seraphin, S. *J. Phys. Chem. Solids* **2000**, *61*, 1055.
(27) Chen, P.; Zhang, H.-B.; Lin, G.-D.; Hong, Q.; Tsai, K. R. *Carbon* **1997**, *35*, 1495.
(28) Kitiyanan, B.; Alvarez, W. E.; Harwell, J. H.; Resasco, D. E. *Chem. Phys. Lett.* **2000**, *317*, 497.
(29) Pinheiro, P.; Schouler, M. C.; Gadelle, P.; Mermoux, M.; Dooryhu, E. *Carbon* **2000**, *38*, 1469.
(30) Liu, S.; Tang, X.; Yin, L.; Koltypin, Y.; Gedanken, A. *J. Mater. Chem.* **2000**, *10*, 1271.
(31) Liu, S.; Tang, X.; Mastai, Y.; Felner, I.; Gedanken, A. *J. Mater. Chem.* **2000**, *10*, 2502.
(32) Liu, S.; Boeshore, S.; Fernandez, A.; Sayagues, M. J.; Fischer, J. E.; Gedanken, A. *J. Phys. Chem. B* **2001**, *105* (32), 7606.
(33) Rana, R. K.; Koltypin, Y.; Gedanken, A. *Chem. Phys. Lett.* **2001**, *344*, 256.
(34) Giamello, E.; Murphy, D.; Ravera, L.; Coluccia, S.; Zecchina, A. *J. Chem. Soc., Faraday Trans.* **1994**, *90*, 3167.
(35) Kijenski, J.; Malinowski, S. *J. Chem. Soc., Faraday Trans.* **1978**, *74*, 250.
(36) Saito, Y.; Yoshikawa, T. *Phys. Rev. B* **1993**, *48*, 1907.
(37) Kiang, C.-H.; Endo, M.; Ajayan, P. M.; Dresselhaus, G.; Dresselhaus, M. S. *Phys. Rev. Lett.* **1998**, *81*, 1869.
(38) Kiskinova, M. P. *Surf. Sci.* **1981**, *111*, 584.
(39) Crowell, J. E.; Garfunkel, E. L.; Somorjai, G. A. *Surf. Sci.* **1982**, *121*, 303.
(40) Campbell, C. T.; Goodman, D. W. *Surf. Sci.* **1982**, *123*, 413.
(41) Jenkins, S. J.; King, D. A. *J. Am. Chem. Soc.* **2000**, *122*, 10610.
(42) Giamello, E.; Ferrero, A.; Coluccia, S.; Zecchina, A. *J. Phys. Chem.* **1991**, *95*, 9385.
(43) Khassin, A. A.; Yurieva, T. M.; Zaikovskii, V. I.; Parmon, V. N. *React. Kinet. Catal. Lett.* **1998**, *64*, 63.
(44) Nikolaev, P.; Bronikowski, M. J.; Bradley, R. K.; Rohmund, F.; Colbert, D. T.; Smith, K. A.; Smalley, R. E. *Chem. Phys. Lett.* **1999**, *313*, 91.
(45) Dillon, A. C.; Gennett, T.; Jones, K. M.; Alleman, J. L.; Parilla, P. A.; Heben, M. J. *Adv. Mater.* **1999**, *11*, 1354.
(46) Ajayan, P. M.; Ebbesen, T. W.; Ichihashi, T.; Iijima, S.; Tanigaki, K.; Hiura, H. *Nature* **1993**, *362*, 512.
(47) Rinzler, A. G.; Liu, J.; Dai, H.; Nikolaev, P.; Huffman, C. B.; Rodriguez-Macias, F. J.; Boul, P. J.; Lu, A. H.; Heymann, D.; Colbert, D. T.; Lee, R. S.; Fischer, J. E.; Rao, A. M.; Eklund, P. C.; Smalley, R. E. *Appl. Phys. A* **1998**, *67*, 29.
(48) Ramirez, A. P.; Haddon, R. C.; Zhou, O.; Fleming, R. M.; Zhang, J.; McClure, S. M.; Smalley, R. E. *Science* **1994**, *265*, 84.
(49) Rieke, R. D. *Chem. Mater.* **1996**, *8*, 1770.
(50) Block, J. A.; Parvin, K.; Alpers, J. L.; Sezen, T.; LaDuca, R. *IEEE Trans. Magn.* **1998**, *34*, 982.
(51) Saito, Y.; Ma, J.; Nakashima, J.; Masuda, M. *Z. Phys. D* **1997**, *40*, 170.